Biomaterials 332 (2026) 124160

Contents lists available at ScienceDirect

Biomaterials

journal homepage: www.elsevier.com/locate/biomaterials

Image-guided optimization of regenerative graft attachment to the heart

Zhiping Feng [a,1], Daniel Hachim [b,c,e,f,1], Ioanna Mylonaki [b,c,f,1], Maria Colzani [d], Annalisa Bettini [a], Camilla Dondi [b,f], Ines Obregon-Gomez [b,g], Junliang Lin [b,c,g,h], Laure Gambardella [d], Semih Bayraktar [d], Emily Deniszczyc [a], Christopher Pope [a], Adama F. Saccoh [a], Ebtehal Ahmed [a], Mark F. Lythgoe [a], Tammy L. Kalber [a], P Stephen Patrick [a], Sanjay Sinha [d], Molly M. Stevens [b,c,f,h,*], Daniel J. Stuckey [a,**]

[a] Centre for Advanced Biomedical Imaging, University College London, UK
[b] Department of Materials, Imperial College London, UK
[c] Institute of Biomedical Engineering, Imperial College London, UK
[d] Cambridge Stem Cell Institute, Jeffrey Cheah Biomedical Centre, University of Cambridge, UK
[e] School of Pharmacy, Faculty of Chemistry and Pharmacy, Pontificia Universidad Católica de Chile, Santiago, Chile
[f] Department of Bioengineering, Imperial College London, UK
[g] Department of Chemistry, Imperial College London, UK
[h] Department of Physiology, Anatomy and Genetics, Department of Engineering Science, Kavli Institute for Nanoscience Discovery, University of Oxford, Oxford, UK

ARTICLE INFO

Keywords:
Cardiac regeneration
Image guidance
Biomaterials
Preclinical models
SPECT

ABSTRACT

Tissue engineering offers great promise for regenerating damaged organs including the heart. Although direct attachment of grafts at the target site is possible during surgery, minimally invasive delivery and suture-free approaches could reduce patient discomfort and allow repeat administration. However, for the therapy to be effective it is essential that the graft is successfully delivered to the epicardium and retained on target.

Here, methacrylated alginate-based shape-memory patches labelled with $^{111}InCl_3$ and loaded with luciferase expressing stem-cells were either injected towards the epicardium under ultrasound guidance or surgically grafted onto mouse hearts. Patch and cell location were serially tracked using SPECT-CT and bioluminescence imaging.

Radiolabelling of shape-memory patches permitted serial tracking of graft location for seven days *in-vivo*, and revealed that injected patches rarely attached on-target whilst surgically implanted patches rapidly detached from the epicardium. *In-vivo* imaging was then used to evaluate modifications to biomaterial formulation and patch attachment strategies. This ultimately resulted in effective, suture-free surgical attachment of chitosan-coated patches loaded with luciferase-expressing human embryonic stem cell-derived epicardial cells onto the heart, illustrating a model therapeutic.

This translational imaging approach facilitates iterative optimization of a novel biomaterial and could have wide-reaching applications for enhancing a range of regenerative therapies.

1. Introduction

Regenerative medicine creates the tantalizing possibility of replacing tissue damaged during myocardial infarction [1]. However, in over 20 years of experimentation, there are few credible reports of substantial cardiac repair [2]. A major reason for this is that even cells with true cardiomyogenic potential are rapidly lost at the time of injection and do not integrate with the host [3,4]. Biomaterials are increasingly used to improve cell retention and viability, and once formulations are optimized, they may finally allow for effective regeneration.

Engineered tissue constructs can support cell survival through

* Corresponding author. Department of Physiology, Anatomy and Genetics, Department of Engineering Science, Kavli Institute for Nanoscience Discovery, University of Oxford, Oxford, UK.
** Corresponding author. Centre for Advanced Biomedical Imaging, University College London, Paul O'Gorman Building, 72 Huntley Street, London, UK, WC1E 6DD.
E-mail addresses: molly.stevens@dpag.ox.ac.uk (M.M. Stevens), d.stuckey@ucl.ac.uk (D.J. Stuckey).
[1] Contributed equally to the manuscript.

https://doi.org/10.1016/j.biomaterials.2026.124160
Received 2 October 2025; Received in revised form 20 March 2026; Accepted 23 March 2026
Available online 24 March 2026
0142-9612/© 2026 The Authors. Published by Elsevier Ltd. This is an open access article under the CC BY license (http://creativecommons.org/licenses/by/4.0/).

Abbreviations

AlgiMA	Alginate methacrylate
AEMA	Amino-ethyl-methacrylamide
APMA	Amino-propyl-methacrylamide
BLI	Bioluminescence imaging
cSMP	chitosan coated shape memory patch
Gen1-SMP	first generation shape memory patch
hESC-epi	Human embryonic stem cell-derived epicardial cells
Luc	firefly luciferase
NSG	NOD-SCID-gamma
NOD-SCID	Non-obese diabetic - severe combined immune deficiency
PEG	Polyethylene glycol
SPECT-CT	Single-photon emission computed tomography - computed tomography

providing a scaffold and enabling cell-cell connections, but they require surgical implantation and mechanical attachment to the heart using sutures or adhesives [5–8]. Clinically approved biomaterials such as alginate and poly-ethylene-glycol can be injected in a minimally invasive fashion and can increase immediate donor-cell retention simply because of their high viscosity [9–11], but do not retain the cell-cell coupling which is vital for regeneration [10]. Recently, much interest has been focused on injectable cell scaffolds, including microspheres [12], organoids [13] and shape memory patches [14] as these offer structured cell delivery vectors which can be administered in a minimally invasive manner and do not require suturing. However, it is essential that the fate of these constructs is monitored to ensure effective on-target delivery and long-term retention at the target organ [4,9,11].

In vivo evaluation of the efficacy of tissue engineered therapies require imaging approaches that can track the location of the graft and the resulting impact on cardiac function. A range of methods have been developed to track therapeutic cells, including reporter genes [15–17] and direct labelling with contrast agents for MRI [18], optical [19] and nuclear imaging [20]. These approaches require modifications to the cell product, which can affect viability and function, potentially to the detriment of the therapy [20,21]. An alternative and less explored approach is to bind contrast agents into the inert biomaterials used to deliver the cell therapy. The approach negates the need for incorporation of potentially toxic agents into cells, but still permits serial tracking of tissue graft location *in vivo*, allowing confirmation of on-target delivery and retention [11]. MRI [6,22], X-ray/CT [12,23], optical [24] and photoacoustic imaging [25,26] have been used to track biomaterials, but all have disadvantages, including lack of specificity, need for high concentration of contrast agent, and poor tissue penetration, respectively. Radionuclide imaging with PET or SPECT provides high sensitivity 3D tracking of clinically approved radiotracers. When combined with high-resolution anatomical information generated by CT, radionuclide imaging offers an ideal platform for 3D quantification of on-target biomaterial retention and whole-body biodistribution.

Here, we developed a rapid and sensitive multimodal imaging method to track the location of therapeutic biomaterials and cells serially *in vivo*, then use these data to modify material formulation and iteratively optimize attachment of cell-seeded patches to the epicardium of mouse hearts.

2. Methods

A detailed methodology is described in the Supplementary Materials.

3. Results

3.1. Shape memory patch (SMP) synthesis and characterization

First generation SMPs were fabricated via cryogelation by cross-linking of alginate methacrylate (AlgiMA) and PEG-diSH through free radical polymerization under freezing conditions, a modified procedure from Bencherif [14], with PEG chains integrated into the polymer networks rather than the side chains. Shape-memory function was only possible when PEG was present, with pure AlgiMA patches not showing shape-memory. During cryogelation, most of the solvent (water) froze, concentrating the dissolved solutes in small semi-frozen liquid microphase regions. Free-radical polymerization and gelation occurred in these regions. After complete polymerization and subsequent incubation at room temperature with washing to remove unreacted precursors, the ice crystals melted and formed interconnected pores (Fig. 1a). An amino-propyl-methacrylamide (APMA) was grafted into the carboxylic acid side-groups of alginate, using EDC/NHS chemistry (Sup. Fig. 1a). APMA was used rather than previously reported amino-ethyl-methacrylamide (AEMA), due to the increased purity of the reagent, which resulted in more reproducible SMP fabrication. ^{1}H NMR showed 45% methacrylation of the AlgiMA product (Sup. Fig. 1b), with a yield >95%. Scanning electron microscopy of an 8 x 8 × 0.5 mm SMP show a dense network of interconnected pores with a size of approximately 60 μm in the smallest dimension, and 200 – 400 μm in the largest dimension (Fig. 1b).

Cryogel patches exhibited shape-memory properties. Square 8 x 8 × 0.5 mm patches passed through 16 and 18-gauge needles and recovered their shape, while 4 x 4 × 0.5 mm patches passed through 19 and 21-gauge, and 2 x 2 × 0.5 mm patches through a 23-gauge needle (Fig. 1c). This shape-memory behavior was also observed via rheology. Patches exhibited a rapid decrease in loss modulus and an increase in storage modulus under low strain conditions, allowing patches to collapse rapidly under low deformation stress (Fig. 1d).

3.2. Shape memory patches can be labelled with ^{111}In to allow tracking using SPECT

Gen1-SMPs were successfully labelled with $^{111}InCl_3$. Saline incubation buffer gave higher initial loading than HEPES buffer (Fig. 2a). Incubation with the strong indium chelator DTPA as a negative control to compete for binding, reduced indium retention to background levels (Fig. 2a). A labelling efficiency of 50% activity retention was achieved after two washes and predicted to be sufficient for *in vivo* imaging owing to the high sensitivity of SPECT for detecting focal points of activity, with our previous data demonstrating that ^{111}In lost from alginate is rapidly cleared from the implantation site [11].

3.3. Ultrasound guided injection of gen1-SMPs did not deliver patches to the target site on the mouse epicardium

Ultrasound-guided injections of *gen1*-SMPs were performed to deliver the patch to the epicardium of 10 mice. SPECT-CT was acquired 1-h post-injection to confirm delivery. In one mouse, the SMP could be visualized as a clearly defined hotspot on SPECT at the target site of the anterior wall (delineated from co-registration with CT). However, in all other animals the patch was off-target, either at the inferior wall of the heart or within the lung-field (Fig. 2b) indicating that ultrasound guided injection of *gen1*-SMPs towards mouse hearts was not an effective delivery route. SPECT-CT repeated at days 1 and 4 was able to serially track SMP location (Fig. Supp3).

3.4. Direct surgical application of gen1-SMPs did not result in retention of patches at the target site

To determine whether the low level of on-target patch delivery was

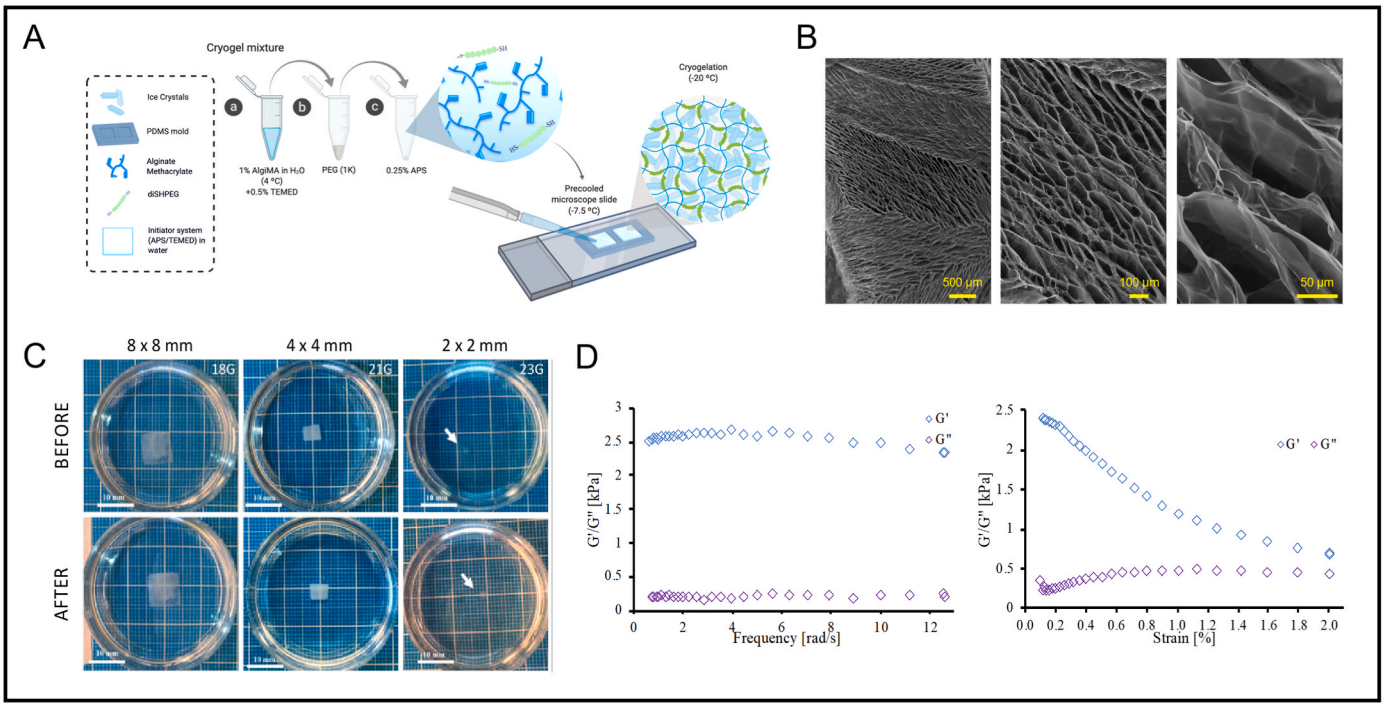


Fig. 1. Patch synthesis and characterization. A) Shape-memory patches (SMP) fabricated via cryogelation. (B) Scanning electron microscopy to visualize patch pore size. (C) Images of SMPs before and after passing through a needle. Needle gauge shown is the smallest which preserves integrity of 8 x 8, 4 x 4 and 2 × 2 mm patches. Bars represent 10 mm. (D) Frequency-sweep tests using increasing frequency with constant shear (0.1%) (left) and strain linear ramp tests using constant frequency (0.6 rad/s) with increasing shear strain (right). Circular samples (8 mm in diameter) were used, most representative sample shown.

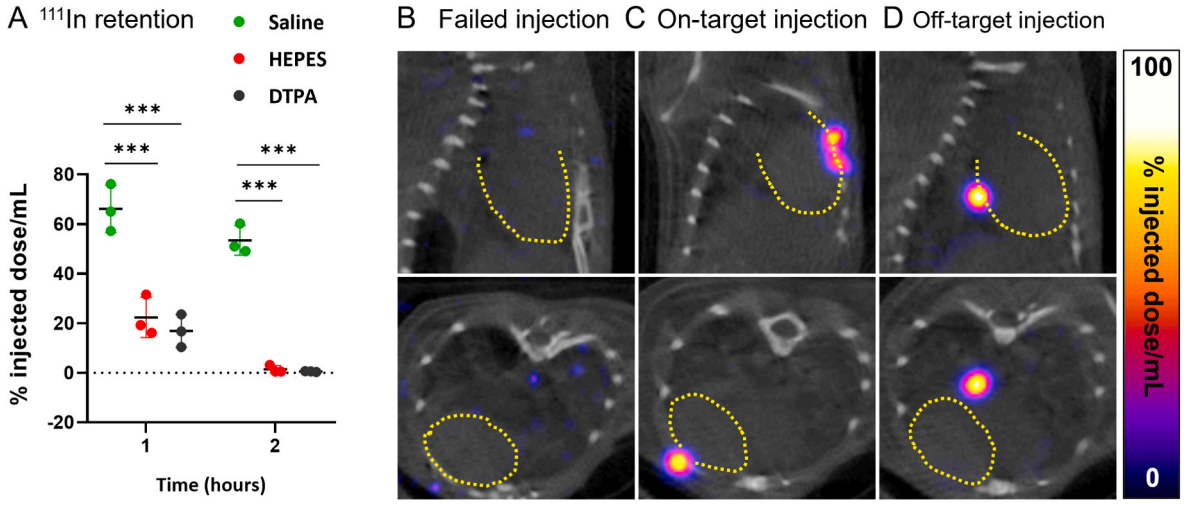


Fig. 2. Ultrasound guided injection of *gen1*-SMPs did not deliver patches to the target site on the mouse epicardium. (A) Retention of ^{111}In after dialysis using saline, HEPES and DTPA. SMP dialyzed against saline exhibited significant higher retention of ^{111}In than HEPES and DTPA. ***$P < 0.0001$. n = 3. error bars = S.D. (B-D) *In vivo* sagittal and axial SPECT-CT of mice 1 h after ultrasound-guided injection of ^{111}In labelled *gen1*-SMPs. Images highlight; (B) failed injection where the patch was not detected; (C) on-target SMP delivery to the anterior myocardium; (D) off-target delivery with the SMP located at the inferior region of the heart. Only 1 of 10 patches successfully attached to the anterior epicardium. Contours of the hearts are delineated by yellow dashed lines. SMP = shape memory patch. (For interpretation of the references to colour in this figure legend, the reader is referred to the Web version of this article.)

due to the ultrasound-guided injection protocol or an inability of SMPs to adhere to the epicardium, radiolabeled *gen1*-SMPs were placed directly onto the heart during open-chest surgery. Visual observations during thoracotomy identified that SMPs were not tightly adhered to the epicardium and could move during contraction. SPECT-CT indicated that within 24 h of implantation SMPs had detached from the epicardium of all 5 mice (Fig. Supp4).

3.5. *Encapsulating gen1-SMPs under a surgical mesh did not enhance on-target delivery*

In an attempt to prevent SMPs from attaching to the internal rib cage as opposed to the epicardium, surgical mesh was positioned on top of the heart and patch before the rib-cage was sealed (n = 4). SPECT-CT indicated that within 24 h of implantation SMPs had detached from the epicardium of all 4 mice (Fig. 3a). SPECT-CT repeated at day 4 and day 7 was able to serially track SMP location (Fig. 3a).

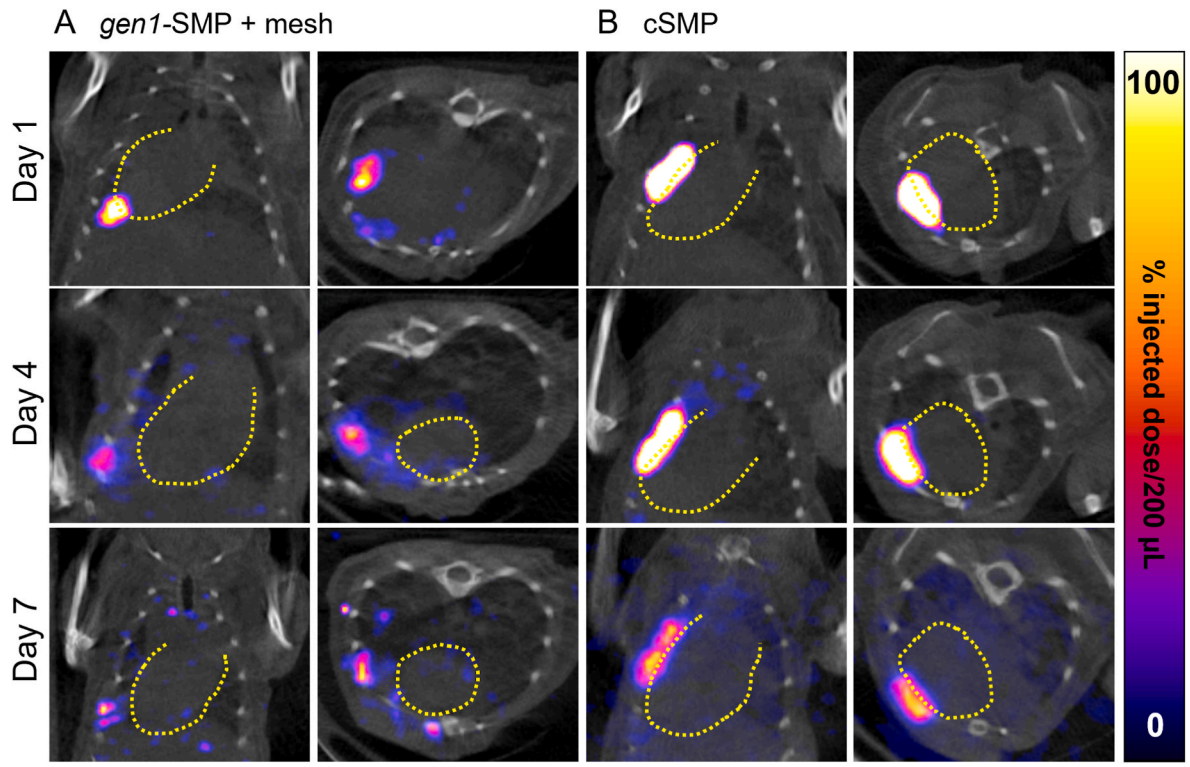


Fig. 3. *gen1*-SMPs encapsulated under a surgical mesh did not enhance on-target delivery whilst cSMPs, modified with a chitosan coating, enhanced on-target delivery. *In vivo* coronal and axial SPECT-CT imaging of (A) ^{111}In labelled *gen1*-SMP attached under a surgical mesh covering showed patch detachment from day 1 (n = 4). (B) ^{111}In labelled cSMP demonstrated stable attachment to the anterior epicardium over 7 days (n = 4). SMP = shape memory patch. cSMP with chitosan coating.

3.6. cSMPs modified with a chitosan coating enhanced on-target delivery

As *gen1*-SMPs clearly were not sufficiently adhesive to remain on the myocardium, we coated patches with chitosan which has been shown to adhere to tissues and is able to adapt to the dynamic tissue movements [27]. These second generation SMPs (cSMP) were radiolabeled and placed directly onto the hearts of 4 mice via open-chest surgery. SPECT-CT indicated that 24 h after implantation cSMPs remained attached to the epicardium of all 4 mice (Fig. 3b). SPECT-CT repeated at day 4 and day 7 was able to serially track cSMP location and confirmed that they remained on-target (Fig. 3b). cSMPs retained more radioactivity than *gen1*-SMPs both *in vitro* and *in vivo* (Fig. Supp5)

3.7. SMPs loaded with hESC-epi cells preserved viability and supported migration in vitro

Human embryonic stem cell-derived epicardial cells (hESC-epi) [28] were seeded onto SMPs and monitored over 4 days using the Incucyte® S3 system. Phase-contrast images (Fig. Supp6A) show significant cell migration *in vitro* from the patches over time. The area covered by migrating cells increased linearly (Fig. Supp6B) with a strong correlation between time and confluence ($R^2 = 0.9794$). Higher magnification images (Fig. Supp6C) confirm the steady migration observed at 0, 24, and 48 h.

Cell viability was assessed using the Live/Dead™ assay (Fig. Supp7). Live cells (green) were predominant across Days 1, 2, and 5, indicating sustained viability and proliferation. The 3D reconstructions further demonstrate uniform cell distribution and health. The negative control of H_2O_2 treated cells confirmed assay specificity, showing mostly dead cells (red).

These results confirm the patches support both migration and sustained viability of hESC-epi, highlighting their potential as a delivery vector for regenerative cells.

3.8. cSMPs loaded with luciferase expressing hESC-epi stably attached to the epicardium and could be serially tracked in vivo

To enable non-invasive *in vivo* viability tracking, hESC-epi were transfected with a lentivirus containing firefly luciferase. cSMPs were labelled with $^{111}InCl_3$, and loaded with luc$^+$ hESC-epi cells 24 h prior to transplant. cSMPs were placed directly onto the heart via open-chest surgery. Immunocompromised NSG (NOD-SCID-gamma) mice received either radiolabeled cSMPs loaded with hESC-epi (n = 6), or radiolabeled cSMPs without cells (n = 4). SPECT-CT acquired 1-h post-implantation confirmed on-target delivery of all 10 patches. SPECT-CT repeated at day 1 and 7 allowed serial tracking of cSMP location and confirmed stable attachment to the epicardium (Fig. 4a). Bioluminescence imaging performed 1 h, 1, 4 and 7 days after implantation confirmed hESC-epi remained viable and within the vicinity of the graft (Fig. 4b). Echocardiography acquired 7 days after implantation found no differences in cardiac structure or function when compared with 7 control NSG mice (Table.Supp1). *Ex vivo* autoradiography (Fig. 4c) and histology (Fig. 5) performed at sacrifice confirmed cSMPs remained attached to the epicardium of the hearts and that nuclei where present within the cell loaded patches.

4. Discussion

Improving the precision of treatment delivery is arguably the greatest unmet need we have in modern medicine [29,30]. Off-target effects often result in undesirable toxicities for patients and their associated cost burden healthcare systems. Biomaterials are increasingly used for targeting therapies and can augment local drug or cell delivery whilst reducing harms associated with traditional treatments [9,31]. However, for this approach to be effective it is essential that materials are delivered and retained on-target. Multi-modality imaging is emerging as a translational tool for not only tracking delivery of

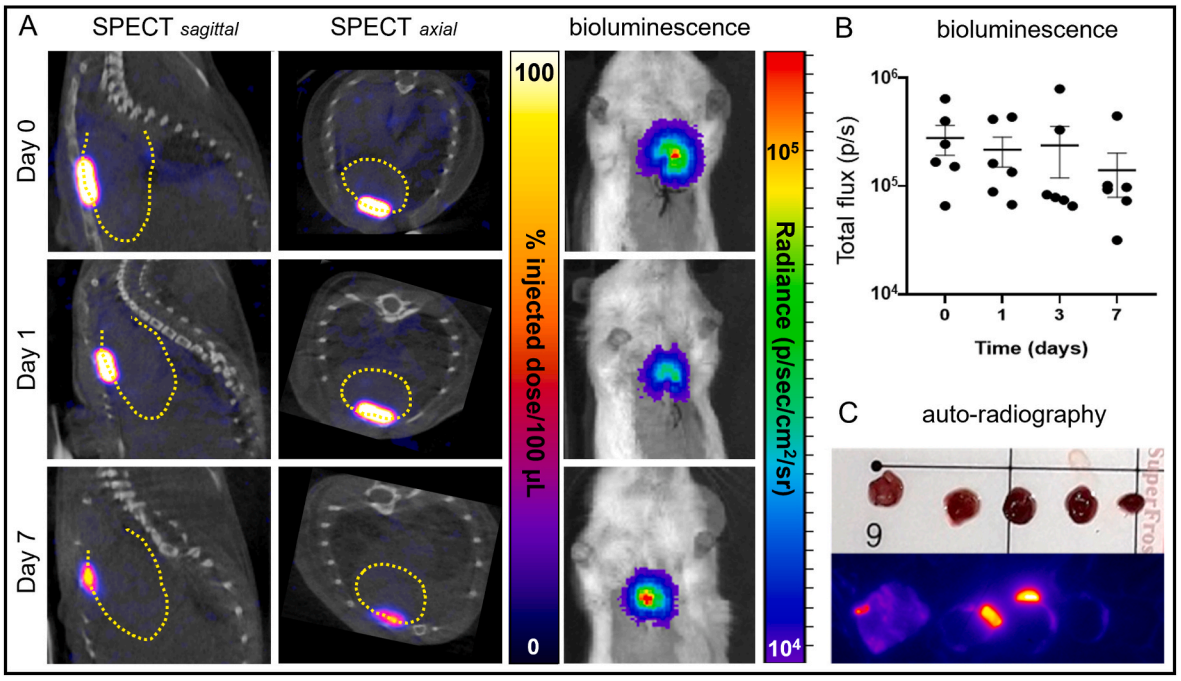


Fig. 4. cSMPs loaded with luciferase $^{+}$ hESC-epi cells stably attached to the epicardium and could be serially tracked *in vivo*. (A) SPECT-CT (left) and BLI (right) on day 0, 1 and 7 following ^{111}In labelled, hESC-epi loaded cSMP implantation. All 10 patches attached onto the hearts for 7 days. (B) BLI signals remained constant over 7 days indicating stable engraftment of 6 hESC-epi loaded cSMPs. Error bars = S.D. (C) *ex vivo* autoradiography confirmed cSMP attachment to the epicardium of the heart. BLI, bioluminescence imaging. cSMP, chitosan coated shape memory patch. hESC-epi, human embryonic stem cell-derived epicardial cells.

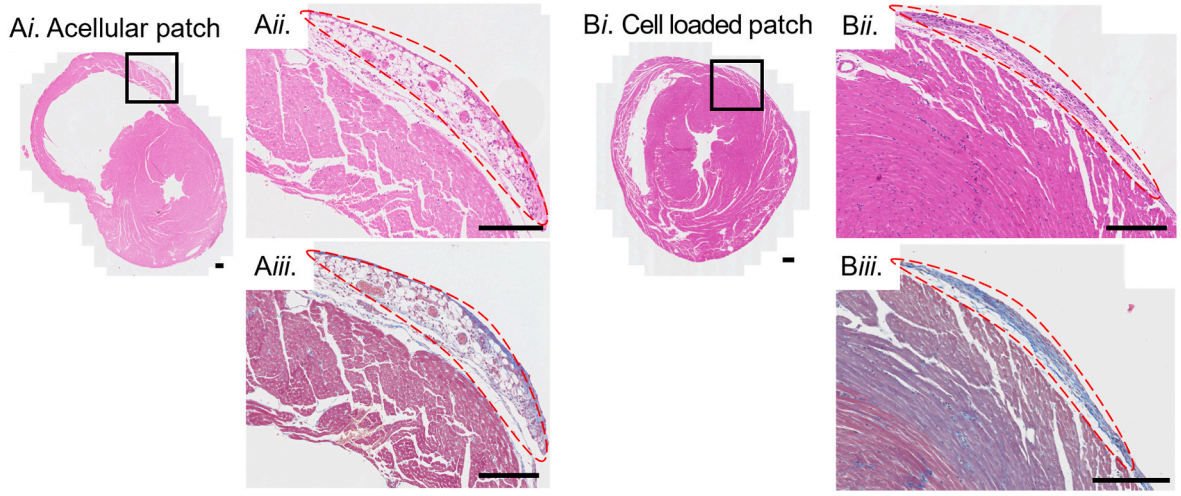


Fig. 5. Representative histology of cSMPs (red dotted lines) attached to the heart. (A) Acellular patch and (B) hESC-epi cell loaded patch on the epicardium of the heart. Sections were stained with (i-ii) hematoxylin and eosin and (iii) Masson's trichrome. Scale bars represent 200 µm. hESC-epi, human embryonic stem cell-derived epicardial cells. (For interpretation of the references to colour in this figure legend, the reader is referred to the Web version of this article.)

therapeutic drugs and cells [20,32,33], but also for visualizing biomaterials and their payloads [12,23,34,35]. Image-guidance has already proved essential for interventional procedures including heart-valve replacement [36] and radiotherapy [37]. Here we applied an image-guided approach to enhance biomaterial graft retention on the heart for effective stem cell delivery which could ultimately enhance regenerative therapies for heart disease [1,3].

Shape memory patches were synthesized, loaded with therapeutic cells and in theory, could be injected onto target organs without the need for invasive surgery. To confirm whether injections were successful, we developed methods to visualize both the SMP and the therapeutic cells after their administration to live mice. Data highlighted the challenges associated with injecting SMPs, with only one of ten patches remaining on target. One reason for this failure was that the liquid required to propel the SMP from the needle, instantly washed the patch from the target site. Although hydrogels and mechanical methods were tested, these were also unable to effectively inject SMPs. Pilot studies that attempted to inject SMPs onto larger rat hearts also resulted in low on-target delivery (data not shown).

Cell-laden hydrogels have previously been injected using minimally invasive procedures and shown to enhance cell retention on target [9,10], but the viscous nature of gels disrupts the cell-cell connections and tissue structures which can be engineered *in vitro*. Clinically, engineered heart tissues are now being grafted through mini-thoracotomies to allow attachment of structured muscle constructs, though this procedure is still highly invasive [8]. Recent studies have highlighted that cell-laden

microspheres can be injected into the myocardium under ultrasound guidance potentially allowing minimally invasive delivery of structured cell systems [8,12]. We demonstrated that SMPs supported hESC-epi growth and could be injected through an appropriate gauge needle, but further optimization will be needed to make this a viable approach for minimally invasive delivery. Hence, experiments next focused on radiolabeling SMPs so that their surgical attachment to the epicardium could be visualized by SPECT and optimized by modifying formulation.

Methacrylated alginate cryogel patches have previously been shown to remain *in situ* after subcutaneous implantation [38], but here *in vivo* imaging demonstrated that SMP adhesion to the myocardium was weak. SPECT-CT indicated that within 24 h of implantation SMPs had detached from the epicardium of all mice. As SMPs may have been attaching to the adjacent internal rib cage rather than the epicardium, *gen1*-SMPs were covered with surgical mesh to prevent adhesions. SPECT-CT indicated that within 24 h of implantation SMPs had again detached from the epicardium and remained detectable off-target at day 4 and 7.

Next, SMPs were modified using an approach proven to generate tough adhesion to diverse wet surfaces [27]. Tough adhesives have a range of applications including dural membrane closure [39], vascular sealing [40], treating oral lesions [41] and muscle injury [42]. Chitosan has emerged as a potential natural adhesive due to its amino groups providing numerous ionic interactions with negatively charged surfaces [27]. One important requirement for strong adhesion to wet surfaces is that the biomaterial should be able to form covalent bonds with negatively charged tissues, while adapting to the dynamic movement of the organ. By coating SMPs with positively charged chitosan it was predicted that electrostatic interactions would attract the polymer to the myocardium - a negatively charged tissue surface, generating bonds compatible with cardiac motion and able to disperse kinetic energy through the polymer matrix of the patch. Radiolabeled cSMPs were placed directly onto hearts and SPECT-CT confirmed attachment to the epicardium, which was maintained at 1, 4, and 7 days with no detrimental effect on cardiac function.

Having developed a patch which could be faithfully attached to the epicardium without the need for invasive suturing which can damage the myocardium, we evaluated how effective SMPs were at delivering therapeutic cells to the heart. We have previously pioneered the derivation of epicardial cells from hESCs and subsequently shown their potential for cardiac repair [28,43,44]. Physiologically, the epicardial cells sit at the surface of the heart and during embryogenesis they instruct the development and maturation of the myocardium. They also play a crucial role in cardiac tissue regeneration after injury [45,46].

Here, we demonstrate that shape-memory patches are effective in supporting both the migration and sustained viability of hESC-epi *in vitro*. The observed linear migration of cells over four days aligns with previous studies that have highlighted the importance of cellular motility in tissue repair and regeneration, particularly in cardiac tissues where rapid and directed cell migration is crucial for effective healing after injury [44]. 3D confocal image reconstructions of Live/Dead™ stained SMPs demonstrate that hESC-epi not only remain viable but also distribute uniformly across the patch, which is essential for consistent tissue integration and function. This high cell viability is consistent with earlier research showing that the inclusion of a pro-survival cocktail can significantly enhance the survival and function of transplanted cells [47].

hESC-epi were transfected to express firefly luciferase, seeded onto cSMPs and placed on the epicardium. Mice underwent multimodal imaging with whole-body anatomy defined by CT, patch location detected using SPECT and hESC-epi location and viability measured using bioluminescence imaging. All patches remained in position on the epicardium and BLI confirmed epi-hESCs remained in close proximity to the graft site. Light scattering means BLI cannot determine the exact location of luciferase expressing cells *in vivo*, but did confirm sustained cell viability over the 7 days of the experiment.

The ability to rapidly locate grafted biomaterials serially *in vivo* using clinically relevant radiolabeling and 3D whole-body biomedical imaging technology has wide-ranging applications across biomedical engineering [4,9]. This approach could be used to evaluate on-target delivery and degradation of biomaterials used for bone and cartilage regeneration, pulmonary repair, islet transplantation and valve replacement. Contrast agents for MRI [6,22], X-ray/CT [12,23], optical [24] and photoacoustic imaging [25] have been used to locate biomaterials *in vivo*, but these tracking methods lack the sensitivity and specificity of SPECT or PET, and often require complex chemical modification of materials which can change their properties and complicate approval for clinical use. Here we used a rapid and simple method to label alginate patches with clinically approved radionuclides, then demonstrated that SMP location could be tracked to guide the development of suture free attachment to the epicardium.

Translation of this technology will need to address the different size, geometry, and mechanical properties of large animal and human hearts. However, an advantage of alginate-based materials is the ease in which formulation can be modified to alter material properties, allowing elasticity to be tailored to different hearts and degradation rates adjusted for optimal clearance [48]. In addition, we envisage that multiple small 10 × 10 mm SMPs will be used, rather than a single large patch. This simplifies scale-up and allows important cell dose escalation studies to be performed in a similar fashion to the design of the BioVAT-HF hiPSC-CM engineered heart muscle clinical trial [8]. The clinical applicability of SPECT-CT and ^{111}In make them ideal for translational studies. In relation to radiation dose for human studies, our labelling efficiency data indicate that 10 × 10 mm SMPs could readily incorporate 2 MBq of ^{111}In, which would provide a sufficient point source for SPECT detection on clinical systems [49]. Using standard Medical Internal Radiation Dose methodology [50]; implantation of 5 patches (total dose of 10 MBq) with an estimated biological half-life of 72 h would result in an effective whole body radiation dose for a 70 Kg patient of 0.16 mSv - A value substantially lower that the ~13 mSv of a routine rest/stress ^{99m}Tc sestamibi cardiac perfusion scan [51]. Localized absorbed dose for the myocardium is estimated to be 150 mSv - substantially lower than the 10,300 mSv mean heart dose which can result as an off-target consequence of lung cancer radiotherapy [52].

After 25 years of speculation on the use of stem cells to repair damaged hearts, pluripotent stem-cell derived cardiomyocytes, epicardial cells and endothelial cells [53–55] finally offer realistic cardiac regeneration and are just beginning to reach clinical trials [8,56]. Despite the proven *in-vitro* potential of these cells, their *in-vivo* efficacy has been disappointing, mainly due to ineffective delivery methods and the lack of approaches to encourage integration within the host myocardium [1,9,10]. The use of adhesive shape-memory materials allows suture-free attachment of a graft which can conform to tissue defects and provide a supportive environment for cell growth and migration [38]. Image guided optimization of biomaterials can be used to ensure effective and sustained delivery of therapeutics and could be utilized in future clinical trials to ensure that advanced pluripotent cell therapies are not lost in translation [2].

4.1. Study limitations

Although this study highlights how image guidance can be used to optimize the formulation of a novel biomaterial which can be used to deliver therapeutic cells to the heart, there are limitations to the work which will be addressed in future studies. Firstly, patches were grafted onto undamaged hearts. Although our prior experience suggests no differences between patch attachment to undamaged or infarcted hearts [5,9,55,57,58], further studies are required to determine efficiency of attachment to the pathological epicardium and whether myocardial repair can be induced. Secondly, it was not possible to deliver SMPs to the epicardium via minimally invasive ultrasound guided-injections. However, sustained and suture free attachment during open-chest surgery was demonstrated, allowing the injection approach to be tested in a

future therapeutic study. Myocardial electrical conduction and contractile cycling were not directly measured. However, ultrasound data showed no global or regional changes in contractility, and we have previously shown that contractility and conduction velocity are not affected when chitosan patches are attached to myocardial tissue slices [57], suggesting that risks of arrhythmia or increased mechanical load are low. We were unable to perform immunohistochemistry to identify donor cell location at the resolution needed to determine whether hESC-epi remained within the patch or had migrated towards the myocardium. However, the presence of *in vivo* and *ex vivo* bioluminescence signal confirms that donor cells were alive and on the heart. Finally, this study only tracked cells and biomaterials for 7 days *in vivo*. Future studies should track the long-term survival of luciferase expressing cells, whilst the long half-life of ^{111}In; high sensitivity of SPECT; and focal hot-spot from the labelled patches could permit tracking beyond 2 weeks [11]. Importantly, previous studies have demonstrated that short term cell engagement directly relates to long term improvements in cardiac function [59], meaning that serially monitored of cell and patch location over 7 days is sufficient to evaluate the initial on-target delivery and perioperative patch retention which are essential for effective therapies.

5. Conclusion

Multimodal imaging can track the location of therapeutic biomaterials and cells serially *in vivo*. These data were used to guide iterative optimization of patch formulation and ultimately enabled suture-free attachment to the epicardium of the mouse heart. This translational imaging approach can be used for evaluating the efficacy of biomaterial delivery and retention across a range of regenerative therapies.

CRediT authorship contribution statement

Zhiping Feng: Writing – review & editing, Visualization, Formal analysis, Data curation. **Daniel Hachim:** Writing – review & editing, Visualization, Formal analysis, Data curation, Conceptualization. **Ioanna Mylonaki:** Writing – review & editing, Visualization, Supervision, Project administration, Methodology, Investigation, Funding acquisition, Formal analysis, Data curation, Conceptualization. **Maria Colzani:** Writing – review & editing, Visualization, Methodology, Investigation, Formal analysis, Data curation. **Annalisa Bettini:** Investigation, Formal analysis, Data curation. **Camilla Dondi:** Investigation, Formal analysis, Data curation. **Ines Obregon-Gomez:** Investigation, Formal analysis, Data curation. **Junliang Lin:** Investigation, Formal analysis, Data curation. **Laure Gambardella:** Investigation, Formal analysis, Data curation. **Semih Bayraktar:** Investigation, Formal analysis, Data curation. **Emily Deniszczyc:** Investigation, Formal analysis, Data curation. **Christopher Pope:** Investigation, Formal analysis, Data curation. **Adama F. Saccoh:** Investigation, Formal analysis, Data curation. **Ebtehal Ahmed:** Investigation, Formal analysis, Data curation. **Mark F. Lythgoe:** Writing – review & editing, Supervision, Formal analysis, Data curation. **Tammy L. Kalber:** Investigation, Formal analysis, Data curation. **P Stephen Patrick:** Investigation, Formal analysis, Data curation, Conceptualization. **Sanjay Sinha:** Writing – review & editing, Supervision, Resources, Project administration, Methodology, Investigation, Funding acquisition, Data curation, Conceptualization. **Molly M. Stevens:** Writing – review & editing, Supervision, Resources, Project administration, Methodology, Funding acquisition, Data curation, Conceptualization. **Daniel J. Stuckey:** Writing – review & editing, Writing – original draft, Visualization, Validation, Supervision, Software, Resources, Project administration, Methodology, Investigation, Funding acquisition, Formal analysis, Data curation, Conceptualization.

Declaration of competing interest

The authors declare the following financial interests/personal relationships which may be considered as potential competing interests:M. M.S. has invested in, consults for (or is on scientific advisory boards or boards of directors) and conducts sponsored research funded by companies related to the biomaterials field; has filed patent applications related to biomaterials; and has co-founded companies in the biomaterials field. The rest of the authors declare that they have no known competing financial interests or personal relationships that could have appeared to influence the work reported in this paper.

Acknowledgments

Funding sources: D.J.S. British Heart Foundation (BHF) FS/15/33/31608,FS/SBSRF/21/31020,RM/17/1/33377, Wellcome Trust 212937/Z/18/Z. S.*P. and* D.J.S. Medical Research Council (MRC) MR/R026416/1. D.H. European Union's Horizon 2020 Marie Skłodowska-Curie 839111, *Agencia Nacional de Investigación y Desarrollo/Fondecyt de Iniciación* 11240633,CIEN-UC. D.H., M.D., S.H. and M.M.S. BHF RM/17/1/33377,RM/21/290002. M.M.S. BHF RE/13/4/30184, Rosetrees Trust and UK Regenerative Medicine Platform "Acellular/Smart Materials–3D Architecture" MR/R015651/1. M.M.S. and S.S. Kusuma Trust. UK. S.S. and M.C. BHF FS/18/46/33663,RM/17/2/33380,RE/18/1/34212. M. F.L. Cancer Research UK (DRCMDP-Nov24/100005,C7893/A27590); Rosetrees Trust, John Black Charitable Foundation (A2200); MRC (MR/M009092/1,MR/J013110/1); Brain Tumour Charity (QfC_2018_10387).

Appendix A. Supplementary data

Supplementary data to this article can be found online at https://doi.org/10.1016/j.biomaterials.2026.124160.

Data availability

Data will be made available on request.

References

[1] R. Bolli, M. Solankhi, X.L. Tang, A. Kahlon, Cell therapy in patients with heart failure: a comprehensive review and emerging concepts, Cardiovasc. Res. 118 (4) (2022) 951–976.
[2] J.J. Zhang, S.M. Pogwizd, K. Fukuda, et al., Trials and tribulations of cell therapy for heart failure: an update on ongoing trials, Nat. Rev. Cardiol. 22 (5) (2024) 372–385.
[3] R. Madonna, L.W. Van Laake, H.E. Botker, et al., ESC working group on cellular biology of the heart: position paper for cardiovascular research: tissue engineering strategies combined with cell therapies for cardiac repair in ischaemic heart disease and heart failure, Cardiovasc. Res. 115 (3) (2019) 488–500.
[4] P.K. Nguyen, J. Riegler, J.C. Wu, Stem cell imaging: from bench to bedside, Cell Stem Cell 14 (4) (2014) 431–444.
[5] R.J. Jabbour, T.J. Owen, P. Pandey, et al., In vivo grafting of large engineered heart tissue patches for cardiac repair, JCI Insight 6 (15) (2021).
[6] D.J. Stuckey, H. Ishii, Q.Z. Chen, et al., Magnetic resonance imaging evaluation of remodeling by cardiac elastomeric tissue scaffold biomaterials in a rat model of myocardial infarction, Tissue Eng. Part A 16 (11) (2010) 3395–3402.
[7] E. Querdel, M. Reinsch, L. Castro, et al., Human engineered heart tissue patches remuscularize the injured heart in a dose-dependent manner, Circulation 143 (20) (2021) 1991–2006.
[8] A.F. Jebran, T. Seidler, M. Tiburcy, et al., Engineered heart muscle allografts for heart repair in primates and humans, Nature 639 (2025) 503–511.
[9] J.P.K. Armstrong, T.J. Keane, A.C. Roques, et al., A blueprint for translational regenerative medicine, Sci. Transl. Med. 12 (572) (2020).
[10] H.S. O'Neill, L.B. Gallagher, J. O'Sullivan, et al., Biomaterial-enhanced cell and drug delivery: lessons learned in the cardiac field and future perspectives, Adv. Mater. 28 (27) (2016) 5648–5661.
[11] P.S. Patrick, J.C. Bear, H.E. Fitzke, et al., Radio-metal cross-linking of alginate hydrogels for non-invasive in vivo imaging, Biomaterials 243 (2020) 119930.
[12] A. Bettini, P.S. Patrick, R.M. Day, D.J. Stuckey, CT-Visible microspheres enable whole-body in vivo tracking of injectable tissue engineering scaffolds, Adv. Healthcare Mater. 13 (17) (2024) e2303588.

[13] Y. Tan, R.C. Coyle, R.W. Barrs, et al., Nanowired human cardiac organoid transplantation enables highly efficient and effective recovery of infarcted hearts, Sci. Adv. 9 (31) (2023) eadf2898.
[14] M. Montgomery, S. Ahadian, L. Davenport Huyer, et al., Flexible shape-memory scaffold for minimally invasive delivery of functional tissues, Nat. Mater. 16 (10) (2017) 1038–1046.
[15] P.E. de Almeida, J.R. van Rappard, J.C. Wu, In vivo bioluminescence for tracking cell fate and function, Am. J. Physiol. Heart Circ. Physiol. 301 (3) (2011) H663–H671.
[16] P.S. Patrick, J. Hammersley, L. Loizou, et al., Dual-modality gene reporter for in vivo imaging, Proc. Natl. Acad. Sci. USA 111 (1) (2014) 415–420.
[17] C. Ashmore-Harris, M. Iafrate, A. Saleem, G.O. Fruhwirth, Non-invasive reporter gene imaging of cell therapies, including T cells and stem cells, Mol. Ther. 28 (6) (2020) 1392–1416.
[18] D.J. Stuckey, C.A. Carr, E. Martin-Rendon, et al., Iron particles for noninvasive monitoring of bone marrow stromal cell engraftment into, and isolation of viable engrafted donor cells from, the heart, Stem Cell. 24 (8) (2006) 1968–1975.
[19] M.T. Berninger, P. Mohajerani, M. Wildgruber, et al., Detection of intramyocardially injected DiR-labeled mesenchymal stem cells by optical and optoacoustic tomography, Photoacoustics 6 (2017) 37–47.
[20] P.S. Patrick, K.K. Kolluri, M. Zaw Thin, et al., Lung delivery of MSCs expressing anti-cancer protein TRAIL visualised with (89)Zr-oxine PET-CT, Stem Cell Res. Ther. 11 (1) (2020) 256.
[21] L. Kostura, D.L. Kraitchman, A.M. Mackay, M.F. Pittenger, J.W. Bulte, Feridex labeling of mesenchymal stem cells inhibits chondrogenesis but not adipogenesis or osteogenesis, NMR Biomed. 17 (7) (2004) 513–517.
[22] S. Kuddannaya, W. Zhu, J.W.M. Bulte, In vivo imaging of implanted hyaluronic acid hydrogel biodegradation, Methods Mol. Biol. 2394 (2022) 743–765.
[23] C. Flechas Becerra, L.V. Barrios Silva, E. Ahmed, et al., X-Ray visible protein scaffolds by bulk iodination, Adv. Sci. (Weinh.) 11 (10) (2024) e2306246.
[24] X. Lei, B. Yang, J. Chen, et al., Biodegradable polyurethane scaffolds in regeneration therapy: characterization and in vivo real-time degradation monitoring by grafted fluorescent tracer, ACS Appl. Mater. Interfaces 16 (1) (2024) 111–126.
[25] H. Geng, E.J. Lupton, Y. Ma, et al., Hybrid polypyrrole and polydopamine nanosheets for precise Raman/photoacoustic imaging and photothermal therapy, Adv. Healthcare Mater. 12 (27) (2023) e2301148.
[26] D. Hachim, O. Hernandez-Cruz, J.E.J. Foote, et al., Self-doped and biodegradable Glycosaminoglycan-PEDOT conductive hydrogels facilitate electrical pacing of iPSC-Derived cardiomyocytes, Adv. Healthcare Mater. (2025) e2403995.
[27] J. Li, A.D. Celiz, J. Yang, et al., Tough adhesives for diverse wet surfaces, Science 357 (6349) (2017) 378–381.
[28] D. Iyer, L. Gambardella, W.G. Bernard, et al., Robust derivation of epicardium and its differentiated smooth muscle cell progeny from human pluripotent stem cells, Development 142 (8) (2015) 1528–1541.
[29] J. Malicki, The importance of accurate treatment planning, delivery, and dose verification, Rep. Practical Oncol. Radiother. 17 (2) (2012) 63–65.
[30] M.J. Mitchell, M.M. Billingsley, R.M. Haley, et al., Engineering precision nanoparticles for drug delivery, Nat. Rev. Drug Discov. 20 (2) (2021) 101–124.
[31] H. Wang, D.J. Mooney, Biomaterial-assisted targeted modulation of immune cells in cancer treatment, Nat. Mater. 17 (9) (2018) 761–772.
[32] B.M. Helfer, V. Ponomarev, P.S. Patrick, et al., Options for imaging cellular therapeutics in vivo: a multi-stakeholder perspective, Cytotherapy 23 (9) (2021) 757–773.
[33] M. Zaw Thin, H. Allan, R. Bofinger, et al., Multi-modal imaging probe for assessing the efficiency of stem cell delivery to orthotopic breast tumours, Nanoscale 12 (31) (2020) 16570–16585.
[34] K. Paliashvili, A. Popov, T.L. Kalber, et al., Peritumoral delivery of Docetaxel-TIPS microparticles for prostate cancer adjuvant therapy, Adv. Ther. 4 (2) (2021) 2000179.
[35] P.S. Patrick, D.J. Stuckey, H. Zhu, et al., Improved tumour delivery of iron oxide nanoparticles for magnetic hyperthermia therapy of melanoma via ultrasound guidance and (111)In SPECT quantification, Nanoscale 16 (42) (2024) 19715–19729.
[36] H. Baumgartner, V. Falk, J.J. Bax, et al., 2017 ESC/EACTS guidelines for the management of valvular heart disease, Eur. Heart J. 38 (36) (2017) 2739–2791.
[37] D.A. Jaffray, Image-guided radiotherapy: from current concept to future perspectives, Nat. Rev. Clin. Oncol. 9 (12) (2012) 688–699.
[38] S.A. Bencherif, R.W. Sands, D. Bhatta, et al., Injectable preformed scaffolds with shape-memory properties, Proc. Natl. Acad. Sci. USA 109 (48) (2012) 19590–19595.
[39] K.C. Wu, B.R. Freedman, P.S. Kwon, et al., A tough bioadhesive hydrogel supports sutureless sealing of the dural membrane in porcine and ex vivo human tissue, Sci. Transl. Med. 16 (739) (2024) eadj0616.
[40] B.R. Freedman, J.A. Cintron Cruz, P. Kwon, et al., Instant tough adhesion of polymer networks, Proc. Natl. Acad. Sci. USA 121 (9) (2024) e2304643121.
[41] D.T. Wu, B.R. Freedman, K.H. Vining, et al., Tough adhesive hydrogel for intraoral adhesion and drug delivery, J. Dent. Res. 102 (5) (2023) 497–504.
[42] S. Nam, J. Lou, S. Lee, J.M. Kartenbender, D.J. Mooney, Dynamic injectable tissue adhesives with strong adhesion and rapid self-healing for regeneration of large muscle injury, Biomaterials 309 (2024) 122597.
[43] J. Bargehr, L.P. Ong, M. Colzani, et al., Epicardial cells derived from human embryonic stem cells augment cardiomyocyte-driven heart regeneration, Nat. Biotechnol. 37 (8) (2019) 895–906.
[44] L. Gambardella, S.A. McManus, V. Moignard, et al., BNC1 regulates cell heterogeneity in human pluripotent stem cell-derived epicardium, Development 146 (24) (2019).
[45] K.D. Poss, L.G. Wilson, M.T. Keating, Heart regeneration in zebrafish, Science 298 (5601) (2002) 2188–2190.
[46] J. Cao, K.D. Poss, The epicardium as a hub for heart regeneration, Nat. Rev. Cardiol. 15 (10) (2018) 631–647.
[47] M.A. Laflamme, K.Y. Chen, A.V. Naumova, et al., Cardiomyocytes derived from human embryonic stem cells in pro-survival factors enhance function of infarcted rat hearts, Nat. Biotechnol. 25 (9) (2007) 1015–1024.
[48] Q.A. Majid, A.T.R. Fricker, D.A. Gregory, et al., Natural biomaterials for cardiac tissue engineering: a highly biocompatible solution, Front. Cardiovasc. Med. 7 (2020) 554597.
[49] Y. Jin, H. Kong, R.Z. Stodilka, et al., Determining the minimum number of detectable cardiac-transplanted 111In-tropolone-labelled bone-marrow-derived mesenchymal stem cells by SPECT, Phys. Med. Biol. 50 (19) (2005) 4445–4455.
[50] R.W. Howell, B.W. Wessels, R. Loevinger, et al., The MIRD perspective 1999. Medical internal radiation dose committee, J. Nucl. Med. 40 (1) (1999) 3S–10S.
[51] M.C. Williams, C. Stewart, N.W. Weir, D.E. Newby, Using radiation safely in cardiology: what imagers need to know, Heart 105 (10) (2019) 798–806.
[52] M. Kearney, M. Keys, C. Faivre-Finn, et al., Exposure of the heart in lung cancer radiation therapy: a systematic review of heart doses published during 2013 to 2020, Radiother. Oncol. 172 (2022) 118–125.
[53] L. Carpenter, C. Carr, C.T. Yang, et al., Efficient differentiation of human induced pluripotent stem cells generates cardiac cells that provide protection following myocardial infarction in the rat, Stem Cell. Dev. 21 (6) (2012) 977–986.
[54] A. Chow, D.J. Stuckey, E. Kidher, et al., Human induced pluripotent stem cell-derived cardiomyocyte encapsulating bioactive hydrogels improve rat heart function post myocardial infarction, Stem Cell Rep. 9 (5) (2017) 1415–1422.
[55] L. Zwi-Dantsis, B. Wang, C. Marijon, et al., Remote magnetic nanoparticle manipulation enables the dynamic patterning of cardiac tissues, Adv. Mater. 32 (6) (2020) e1904598.
[56] T. Kawamura, Y. Ito, E. Ito, et al., Safety confirmation of induced pluripotent stem cell-derived cardiomyocyte patch transplantation for ischemic cardiomyopathy: first three case reports, Front. Cardiovasc. Med. 10 (2023) 1182209.
[57] M. Kapnisi, C. Mansfield, C. Marijon, et al., Auxetic cardiac patches with tunable mechanical and conductive properties toward treating myocardial infarction, Adv. Funct. Mater. 28 (21) (2018) 1800618.
[58] Q.A. Majid, P. Pandey, M. Bellahcene, et al., Melt electrowritten medium chain length polyhydroxyalkanoate cardiac patches for Post-MI cardiac regeneration, Mater. Today Bio 34 (2025) 102256.
[59] J. Liu, K.H. Narsinh, F. Lan, et al., Early stem cell engraftment predicts late cardiac functional recovery: preclinical insights from molecular imaging, Circ., Cardiovasc. Imaging 5 (4) (2012) 481–490.